Proton tunneling in the dissociation of H_2^+ and its asymmetric isotopologues driven by circularly polarized THz laser pulses

Yidian Tian; Kunlong Liu ✉ iD ; Yuchen Wang; Yueming Zhou iD ; Peixiang Lu
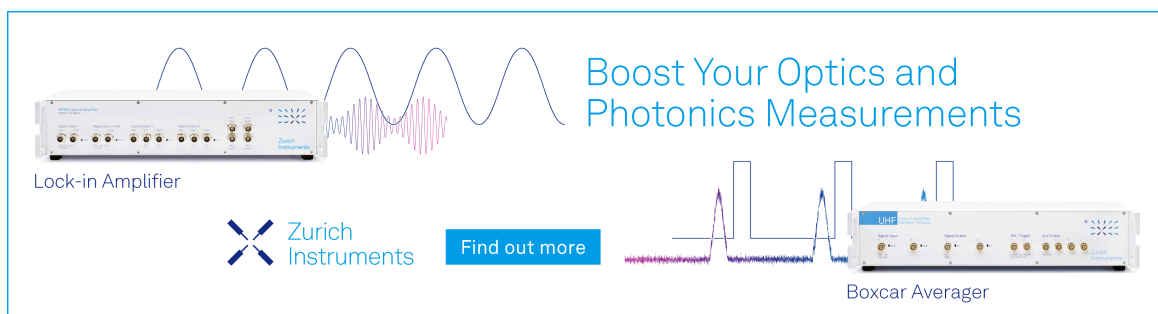
Check for updates

CrossMark

View Online

Export Citation

Proton tunneling in the dissociation of H$_2^+$ and its asymmetric isotopologues driven by circularly polarized THz laser pulses

View Online   Export Citation   CrossMark

Yidian Tian,[1] Kunlong Liu,[1,a] (iD) Yuchen Wang,[1] Yueming Zhou,[1] (iD) and Peixiang Lu[1,2]

AFFILIATIONS

[1] School of Physics and Wuhan National Laboratory for Optoelectronics, Huazhong University of Science and Technology, Wuhan 430074, China
[2] Optics Valley Laboratory, Hubei 430074, China

[a] Author to whom correspondence should be addressed: liukunlong@hust.edu.cn

ABSTRACT

Light-induced deprotonation of molecules is an important process in photochemical reactions. Here, we theoretically investigate the tunneling deprotonation of H$_2^+$ and its asymmetric isotopologues driven by circularly polarized THz laser pulses. The quasi-static picture shows that the field-dressed potential barrier is significantly lowered for the deprotonation channel when the mass asymmetry of the diatomic molecule increases. Our numerical simulations demonstrate that when the mass symmetry breaks, the tunneling deprotonation is significantly enhanced and the proton tunneling becomes the dominant dissociation channel in the THz driving fields. In addition, the simulated nuclear momentum distributions show that the emission of the proton is directed by the effective vector potential for the deprotonation channel and, meanwhile, the angular distribution of the emitting proton is affected by the alignment and rotation of the molecule induced by the rotating field.

Published under an exclusive license by AIP Publishing. https://doi.org/10.1063/5.0195867

I. INTRODUCTION

Deprotonation is one of the fundamental processes in chemical reactions. It is the removal of a proton from a molecule, which is the first step of the proton transfer occurring in proteins, enzymes, and proton channels.[1–3] Deprotonation is also an important process in the photoelectrochemical water splitting for the production of renewable hydrogen.[4,5] Here, to explore the physical mechanisms for increasing the reactivity of molecular deprotonation under radiation, we theoretically investigate the proton tunneling in molecular dissociation driven by circularly polarized THz laser pulses.

As H$_2^+$ and its asymmetric isotopologues, HD$^+$ and HT$^+$, are the most elementary molecular systems in nature, their fragmentation driven by lasers constitutes an ideal prototype reaction for understanding the deprotonation in more complex chemical reactions. The mechanisms of H$_2^+$ fragmentation in laser fields have been widely investigated during the past few decades.[6–19] The so-called bond-softening[15] and above-threshold dissociation[16] are two typical mechanisms for removing a proton from H$_2^+$ with infrared laser fields, where the molecule is stretched to critical internuclear distances and then dissociates into a neutral atomic hydrogen and a proton via net-absorbing the photon energy. However, the reactivity under these two mechanisms significantly declines when the nuclear mass increases[20] because heavier nuclei are less likely to reach the internuclear distances for the resonant excitation.

Another mechanism for molecular dissociation is the nuclear tunneling. Quantum tunneling of nuclei is increasingly found to play an important role in many chemical transformations.[21–23] It has been shown that nuclear tunneling changes reaction paths,[24] lowers the necessary energy for chemical reactions,[25] and enables distinct reactivity modes.[26] In a previous theoretical study, Li et al. focused on the dissociation of H$_2^+$ driven by THz fields and demonstrated the evidence of tunneling dissociation by showing the dissociation probability of the molecule in different initial vibrational states.[17] Yet, due to the limitation of their theoretical model, only linearly polarized driving fields and symmetrical molecular ions were considered. As circularly polarized laser pulses are commonly used to drive and control the tunneling electrons from atoms in the studies of

strong-field ionization,[27,28] it is appealing to ask whether and how a proton could be removed from a molecule under the tunneling mechanism of dissociation driven by circularly polarized laser fields.

To address this question, in the present work, we investigate the tunneling mechanism of the deprotonation process of H_2^+ and its *asymmetric* isotopologues (HD^+ and HT^+) driven by circularly polarized THz laser fields. We numerically solve the time-dependent Schrödinger equation (TDSE) for the two-dimensional two-level model of the diatomic molecular systems, in which the rotation of the molecules during interactions with the circularly polarized fields is taken into account. It is found that for the THz fields of given pulse intensities, the probability of tunneling deprotonation increases exponentially as the degree of the mass asymmetry of diatomic molecules increases. We also demonstrate that the dependence of the tunneling deprotonation on the mass asymmetry and pulse intensity differs essentially from that in the multiphoton dissociation regime. In addition, we show the simulated nuclear momentum distributions for HD^+ induced by the circularly polarized THz laser fields and further discuss the effect of molecular rotation on the tunneling deprotonation.

II. THEORETICAL MODEL

Considering the molecular system of one electron and two nuclei of the same charge, the TDSE is written as (in atomic units)[18]

$$i\frac{\partial}{\partial t}\Phi(\mathbf{R},\mathbf{r},t) = \big[\hat{T}_N + \hat{T}_e + V_{eN}(\mathbf{R},\mathbf{r}) + V_{NN}(\mathbf{R}) + V_t(t)\big]\Phi(\mathbf{R},\mathbf{r},t), \quad (1)$$

where $\mathbf{r}$ is the coordinate of the electron with respect to the center of mass and $\mathbf{R}$ is defined as the distance vector pointing from the heavier nucleus (referred to as the left core) to the other one (referred to as the right core). For the rest of the Hamiltonian terms, $\hat{T}_N$ and $\hat{T}_e$ denote the nuclear and electronic kinetic energy, respectively, $V_{eN}(\mathbf{R},\mathbf{r})$ denotes the Coulomb interaction of the electron with the nuclei, $V_{NN}(\mathbf{R})$ denotes the Coulomb interaction between

two nuclei, and $V_t(t)$ denotes the interaction between the laser field and the molecule, which is given by[18]

$$V(t) = \left[\frac{m_L - m_R}{m_L + m_R}\mathbf{R} + \left(1 + \frac{1}{1 + m_L + m_R}\right)\mathbf{r}\right]\cdot\mathbf{E}(t), \quad (2)$$

with $\mathbf{E}(t)$ being the vector of the electric field and m_L and m_R being the mass of the left (heavier) and right (lighter) cores, respectively.

The full-dimensional simulation of the diatomic molecular ions interacting with the circularly polarized laser fields would require huge computation resources, but we could apply certain approximations according to the practical situations. In the present work, the nuclear motion is restricted in the two-dimensional space. Meanwhile, the linear field intensity is restricted below 10^{14} W/cm^2 to avoid significant ionization and excitation in highly excited electronic states. Under such a condition, the molecular dynamics can be well described in terms of the two lowest-lying electronic states, as demonstrated in many previous studies.[19,30–32] Then, within the Born–Oppenheimer approximation, the wave function can be written as

$$\Phi(\mathbf{R},\mathbf{r},t) = \chi_g(\mathbf{R},t)\phi_g(\mathbf{R},\mathbf{r}) + \chi_u(\mathbf{R},t)\phi_u(\mathbf{R},\mathbf{r}), \quad (3)$$

where $\phi_g(\mathbf{R},\mathbf{r})$ and $\phi_u(\mathbf{R},\mathbf{r})$ represent the wave functions of the electronic eigenstates ($1s\sigma_g$ and $2p\sigma_u$) and $\chi_g(\mathbf{R},t)$ and $\chi_u(\mathbf{R},t)$ denote the corresponding nuclear wave functions. Consequently, we have

$$\big[\hat{T}_e + V_{eN}(\mathbf{R},\mathbf{r})\big]\phi_g(\mathbf{R},\mathbf{r}) = E_1(\mathbf{R})\phi_g(\mathbf{R},\mathbf{r}), \quad (4)$$

$$\big[\hat{T}_e + V_{eN}(\mathbf{R},\mathbf{r})\big]\phi_u(\mathbf{R},\mathbf{r}) = E_2(\mathbf{R})\phi_u(\mathbf{R},\mathbf{r}), \quad (5)$$

where $E_1(\mathbf{R})$ and $E_2(\mathbf{R})$ are the eigenenergies of the electron in the $1s\sigma_g$ and $2p\sigma_u$ states at each internuclear distance, respectively. By submitting Eqs. (1)–(3) and applying Eqs. (2), (4), and (5), one can eventually obtain the following equation set:

$$i\frac{\partial}{\partial t}\begin{pmatrix}\chi_g(\mathbf{R},t)\\\chi_u(\mathbf{R},t)\end{pmatrix} = \begin{pmatrix}\hat{T}_N + V_g(\mathbf{R}) + a_1\mathbf{R}\cdot\mathbf{E}(t) & a_2\mathbf{D}(\mathbf{R})\cdot\mathbf{E}(t)\\a_2\mathbf{D}(\mathbf{R})\cdot\mathbf{E}(t) & \hat{T}_N + V_u(\mathbf{R}) + a_1\mathbf{R}\cdot\mathbf{E}(t)\end{pmatrix}\begin{pmatrix}\chi_g(\mathbf{R},t)\\\chi_u(\mathbf{R},t)\end{pmatrix} \quad (6)$$

with

$$a_1 = \left[-1 + \frac{1}{2}\left(1 + \frac{1}{1 + m_L + m_R}\right)\right]\left(\frac{m_L - m_R}{m_L + m_R}\right) \quad (7)$$

and

$$a_2 = 1 + \frac{1}{1 + m_L + m_R}. \quad (8)$$

Here, $V_g(\mathbf{R}) = E_1(\mathbf{R}) + V_{NN}(\mathbf{R})$ and $V_u(\mathbf{R}) = E_2(\mathbf{R}) + V_{NN}(\mathbf{R})$ are the potential surfaces of the $1s\sigma_g$ and $2p\sigma_u$ states, respectively. $\mathbf{D}(\mathbf{R}) = \langle\phi_g(\mathbf{R},\mathbf{r})|\mathbf{r}|\phi_u(\mathbf{R},\mathbf{r})\rangle$ denotes the transition dipole moment, which is approximately given by[29]

$$\mathbf{D}(\mathbf{R}) = \frac{\mathbf{R}}{\sqrt{4 - 4d_R^2}} \quad (9)$$

with

$$d_R = e^{-|\mathbf{R}|}\left(1 + |\mathbf{R}| + \frac{1}{3}|\mathbf{R}|^2\right). \quad (10)$$

The circularly polarized electric field $\mathbf{E}(t)$ is defined via the vector potential as

$$\mathbf{E}(t) = -\frac{d}{dt}\mathbf{A}(t), \quad (11)$$

where

$$\mathbf{A}(t) = -\frac{E_0}{\omega}\sin^2\left(\frac{\omega t}{2n}\right) \times \left[\sin\left(\omega t + \phi\right)\mathbf{e}_x - \cos\left(\omega t + \phi\right)\mathbf{e}_y\right] \quad (12)$$

with the electric field amplitude E_0, the laser frequency ω, the total number of laser cycles n, and the carrier-envelope phase ϕ ($\phi = 0$ unless stated otherwise). Note that there are the following two main limitations of the present model: (i) the vibration and rotation of the molecule is restricted in the plane of polarization of the laser pulse and (ii) the ionization and the excitation to excited states beyond the first excited state are not included. Therefore, to apply the present model, one should ensure that (i) the nuclear motion beyond the laser polarization plane does not play a key role in the investigation and (ii) the ionization and highly excitation of the systems are neglectable.

In the present study, we numerically solve Eq. (6) with the split-operator method[33] and obtain the time-dependent wave functions $\chi_g(\mathbf{R}, t)$ and $\chi_u(\mathbf{R}, t)$, which describe the nuclear motion on a two-dimensional Cartesian grid (R_x, R_y) in parallel to the polarization plane of the electric field. The grid ranges from -29.975 to 29.975 a.u. in each direction, with the same grid size of $\Delta R_x = \Delta R_y = 0.05$ a.u. The time step for the propagation is 0.1 a.u. The convergence of the simulation has been confirmed with shorter time steps.

The initial ground state is obtained via the imaginary time propagation of the wave function.[34] For real-time propagation, to avoid the nonphysical reflection at the boundary of the simulation grid, the wave functions are, in turn, split into the inner and asymptotic parts as follows:

$$\chi_{g,u}(\mathbf{R}, t) = \chi_{g,u}^I(\mathbf{R}, t) + \chi_{g,u}^A(\mathbf{R}, t)$$
$$= \chi_{g,u}(\mathbf{R}, t)V_s(\mathbf{R}) + \chi_{g,u}(\mathbf{R}, t)[1 - V_s(\mathbf{R})], \quad (13)$$

with the splitting function $V_s(\mathbf{R})$ defined as[35]

$$V_s(\mathbf{R}) = 1 - \left[1 + \exp\left(\frac{-(|\mathbf{R}| - R_s)}{\delta_R}\right)\right]^{-1}, \quad (14)$$

where we set the parameters as $R_s = 21$ a.u. and $\delta_R = 0.9$ a.u. so that the wave functions are smoothly split in the region where the potential is nearly zero. In our calculations, the wave functions are split every 8 a.u. of time.

After the separation, the inner parts $\chi_{g,u}^I(\mathbf{R}, t)$ are kept on propagating numerically under the full Hamiltonian, while the asymptotic parts $\chi_{g,u}^A(\mathbf{R}, t)$ can be propagated analytically.[30] In the asymptotic region, the potential energy $V_{g,u}(\mathbf{R})$ is zero and the transition dipole moment $\mathbf{D}(\mathbf{R})$ diverges as $\mathbf{R}/2$. Thus, the coupled equations in Eq. (6) can be decoupled via introducing the following wave functions:

$$\chi_{\text{R,L}}(\mathbf{R}, t) = \frac{1}{\sqrt{2}}\left[\chi_g^A(\mathbf{R}, t) \pm \chi_u^A(\mathbf{R}, t)\right], \quad (15)$$

where $\chi_{\text{R,L}}$ are the nuclear wave functions indicating that the electron is localized on the right (lighter) and left (heavier) nuclei, respectively. The time evolution of $\chi_{\text{R,L}}(\mathbf{R}, t)$ is then given by

$$i\frac{\partial}{\partial t}\chi_{\text{R,L}} = \left[\hat{T}_N + \left(a_1 \pm \frac{a_2}{2}\right)\mathbf{R} \cdot \mathbf{E}(t)\right]\chi_{\text{R,L}}. \quad (16)$$

It can be seen that Eq. (16) is formally analogous to the TDSE (in length gauge) for a free electron driven by the electric field. By applying $\chi_{\text{R,L}}' = e^{-i\mathbf{A}_{1,2}(t)\mathbf{R}}\chi_{\text{R,L}}$ with $\mathbf{A}_{1,2}(t) = (a_1 \pm a_2/2)\mathbf{A}(t)$, Eq. (16) is transformed to

$$i\frac{\partial}{\partial t}\chi_{\text{R,L}}' = \frac{1}{2\mu}[\hat{\mathbf{p}}_N + \mathbf{A}_{1,2}(t)]^2\chi_{\text{R,L}}', \quad (17)$$

with $\mu^{-1} = m_{\text{L}}^{-1} + m_{\text{R}}^{-1}$ and $\hat{\mathbf{p}}_N = (-i\partial/\partial R_x, -i\partial/\partial R_y)$. Now that there is no scalar potential term in Eq. (17), one can analytically propagate the wave functions in the momentum space and eventually obtain the momentum distributions of the dissociating nuclear wave packets.[30]

III. RESULTS AND DISCUSSION

When molecules are exposed to laser fields, the molecular potential curves (or potential surfaces) can be dressed. To obtain an intuitive physical picture of the field-dressed potential curves/surfaces of the diatomic molecules, we calculate the so-called quasi-static states that result from diagonalization of the interaction Hamiltonian given by[29]

$$\hat{H}_{\text{int}}(\mathbf{R}, t) = \begin{pmatrix} V_g(\mathbf{R}) + a_1\mathbf{R} \cdot \mathbf{E}(t) & a_2\mathbf{D}(\mathbf{R}) \cdot \mathbf{E}(t) \\ a_2\mathbf{D}(\mathbf{R}) \cdot \mathbf{E}(t) & V_u(\mathbf{R}) + a_1\mathbf{R} \cdot \mathbf{E}(t) \end{pmatrix}. \quad (18)$$

The resulting quasi-static eigenvalues $V_\pm(\mathbf{R}, t)$ are

$$V_\pm(\mathbf{R}, t) = \frac{V_g(\mathbf{R}) + V_u(\mathbf{R})}{2} + a_1\mathbf{R} \cdot \mathbf{E}(t)$$
$$\pm \sqrt{\frac{[V_g(\mathbf{R}) - V_u(\mathbf{R})]^2}{4} + [a_2\mathbf{D}(\mathbf{R}) \cdot \mathbf{E}(t)]^2}. \quad (19)$$

One can see from Eq. (19) that the field-dressed potentials depend not only on the electric field but also on the parameter a_1 that is determined by the asymmetry of the nuclear masses [see Eq. (7)]. In Fig. 1(a), we show the field-dressed potential curves $V_\pm(R_x; R_y = 0)$ of H_2^+, HD^+, and HT^+ under the electric field pointing at $\mathbf{e}_x$. The field-dressed potential surfaces $V_-(\mathbf{R})$ of H_2^+ and HT^+ are also shown in Figs. 1(b) and 1(c), respectively. One can see that the $1s\sigma_g$ potential curves/surfaces are bent by the external field and the potential barriers with finite height along the field direction are formed. In such a case, if the electric field changes slowly enough with respect to the nuclear motions, there would be a possibility for the nuclear wave packet tunneling through the barrier,[17] as indicated by the horizontal dotted arrows shown in Fig. 1. Interestingly, the formation of the barriers is affected by the nuclear mass. For instance, the potential surface for H_2^+ is symmetrically bent [see Fig. 1(b)], whereas for the asymmetric molecules, the potential barriers to the dissociation channels on the left-hand side ($HD^+ \rightarrow H + D^+$ and $HT^+ \rightarrow H + T^+$) are much thicker than those on the right-hand side ($HD^+ \rightarrow D + H^+$ and $HT^+ \rightarrow T + H^+$). It indicates that the tunneling of the proton would be easier compared to the tunneling of the heavier nucleus from the molecule. On the other hand, by comparing the potential barriers of H_2^+, HD^+, and HT^+ on the right-hand side of Fig. 1(a), one can see that the barrier becomes shorter and
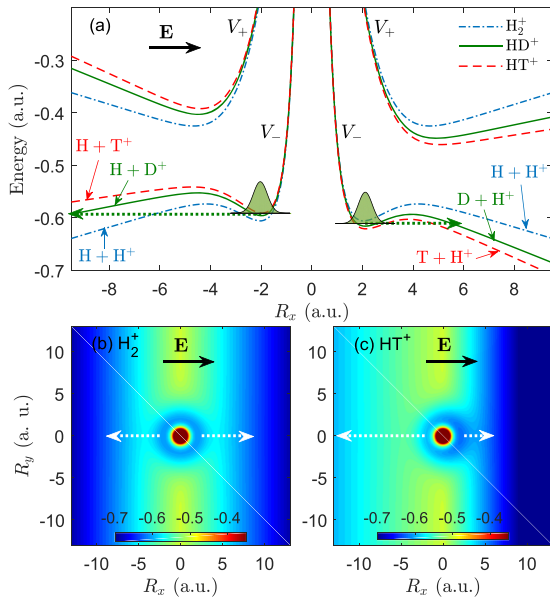
FIG. 1. (a) Field-dressed quasi-static potential curves $V_\pm(R_x;\ R_y = 0)$ of H_2^+ and its isotopologues. (b) Field-dressed quasi-static potential surface V_- of H_2^+. (c) Field-dressed quasi-static potential surface V_- of HT^+. The thick solid arrows indicate the polarization of the electric field. The dotted arrows indicate the tunneling dissociation channels through the barriers. The field amplitude used for the calculation is $|\mathbf{E}| = 0.0292$ a.u.

lower for heavier asymmetric isotopologue. It suggests that the proton tunneling would be easier if the other nucleus of the molecule is heavier. In particular, the potential barrier to the dissociation channel $T + H^+$ is so small [see Fig. 1(c)] that tunneling deprotonation is expected to take place easily even if the electric field is weak.

To study the tunneling dissociation affected by the nuclear mass as discussed above, we numerically solve Eq. (6) and calculate the dissociation probabilities for an artificial molecule, HX^+, driven by the circularly polarized THz pulse with the wavelength of 46 000 nm. Here, the letter X indicates the nucleus with the electric charge of +1 a.u. and the mass of m_x varying from one to three times the proton's mass m_p. The total dissociation yields under the three pulse intensities are shown in Fig. 2. The data for Figs. 2(a) and 2(b) are the same but they are shown on the linear and logarithmic scales, respectively. It is shown that as the nucleus X gets heavier, the dissociation probability increases exponentially until the dissociation eventually approaches saturation. Such phenomenon seems counterintuitive, as heavier molecules are expected to dissociate with a lower probability under the infrared laser pulses.[20] In fact, this seeming contradiction is due to the distinct underlying dissociation mechanisms that are classified with the dissociation adiabaticity parameter,[36]

$$\gamma_N = \sqrt{\frac{2D_p}{U_N}}, \qquad (20)$$

where D_p is the potential energy for dissociation and $U_N = E_0^2/(4\mu\omega^2)$ is the nuclear ponderomotive energy. The dissociation
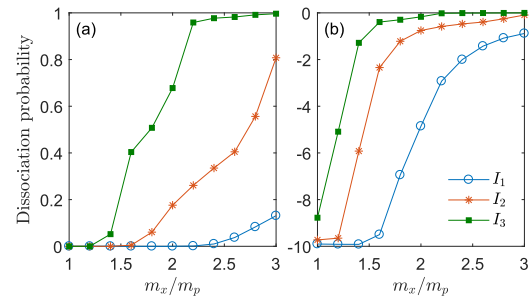

FIG. 2. Dissociation probability of HX^+ as a function of the mass ratio m_x/m_p under three intensities ($I_1 = 4 \times 10^{13}$ W/cm^2, $I_2 = 6 \times 10^{13}$ W/cm^2, and $I_3 = 8 \times 10^{13}$ W/cm^2) of the three-optical-cycle circularly polarized THz pulse. The pulse wavelength is 46 000 nm. The data are shown on the linear and logarithmic scales for (a) and (b), respectively. The total dissociation probability of HX^+ is defined as $P = P_{X+H^+} + P_{H+X^+} = \int |\chi'_L(p_x, p_y; t = t_f)|^2 \, dp_x dp_y + \int |\chi'_R(p_x, p_y; t = t_f)|^2 dp_x dp_y$. In addition, m_x and m_p denote the mass of the artificial nucleus X and the proton, respectively.

is considered to be in the multiphoton regime when $\gamma_N \gg 1$ and in the tunneling regime when $\gamma_N \lesssim 1$.

For infrared driving pules where $\gamma_N \gg 1$, the dissociation is dominated by multiphoton excitation. As the heavier nuclei are less likely to be driven to the internuclear distances for resonant excitation, the dissociation yield would decline with increasing nuclear mass. Figures 3(a) and 3(b) show the probabilities of two dissociation channels (P_{X+H^+} and P_{H+X^+}) of HX^+ driven by the circularly polarized infrared and THz pulses, respectively. For the 800-nm pulse, as expected, the total dissociation probability declines with increasing m_x. Meanwhile, the probability of removing the proton from the molecule is almost equal to that of removing the nucleus X^+, as shown in Fig. 3(a). In this case, the dipole moment of the asymmetric molecule only leads to slightly different probabilities between the two dissociation channels.

In contrast, for the 46 000-nm pulse where $\gamma_N < 1$, the nuclear tunneling dominates the dissociation. As shown in Fig. 3(b), as the
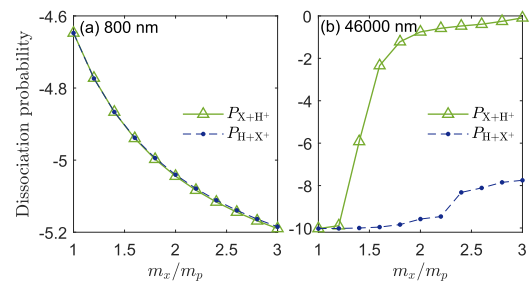

FIG. 3. Dissociation probability of the two channels ($HX^+ \to H + X^+$ and $HX^+ \to X + H^+$) as a function of the mass ratio m_x/m_p under the laser pulses with wavelengths of 800 nm (a) and 46 000 nm (b). The probabilities for the two dissociation channels are calculated by $P_{X+H^+} = \int |\chi'_L(p_x, p_y; t = t_f)|^2 dp_x dp_y$ and $P_{H+X^+} = \int |\chi'_R(p_x, p_y; t = t_f)|^2 dp_x dp_y$, respectively. The field amplitudes are 0.0506 and 0.0292 a.u. for the ten-optical-cycle circularly polarized infrared pulse and the three-optical-cycle circularly polarized THz pulse, respectively. The data are shown on logarithmic scales.

symmetry of the molecule breaks, the probability of dissociation into $X + H^+$ is higher than that of $H + X^+$ by a few orders. This is because the potential barrier to the $X + H^+$ channel is significantly lower than that to $H + X^+$ for the asymmetric molecules where $m_x > m_p$, as shown in Fig. 1. Moreover, the results in Fig. 3(b) show that the probability of the dissociation channel $X + H^+$ increases significantly with increasing m_x. This can also be understood from Fig. 1(a), which shows that the potential barrier to the $X + H^+$ channel becomes lower for heavier isotopologues. Therefore, the observation of the dissociation yields agrees with the physical picture regarding the nuclear wave packet tunneling through the field-dressed quasi-static potentials shown in Fig. 1. So far, our numerical results demonstrate that (i) the removal of the proton from the molecule is the dominant dissociation channel of the asymmetric diatomic molecule in the THz fields and (ii) the corresponding reactivity becomes even higher if the degree of the mass asymmetry of the molecule is larger.

To explore more features of the nuclear tunneling mechanism, we investigate the dependence of the deprotonation of H_2^+, HD^+, and HT^+ on the intensity of the THz laser pulse. The calculated deprotonation yields as a function of the pulse intensity are shown in Fig. 4(a). For comparison, Fig. 4(b) also shows the results for the infrared driving pulse. One can see the distinct intensity dependence of the deprotonation between the multiphoton and tunneling regimes of the dissociation. For the 800-nm driving pulse, the deprotonation yield grows exponentially as the pulse intensity increases exponentially, and the trends for the three molecules are similar in general. For the 46 000-nm driving pulse, however, the trends appear differently. As the pulse intensity increases, the deprotonation for three molecules stays low at first, but then it is enhanced abruptly at different critical intensities and eventually approaches saturation. In this case, the overall probability of the dissociation under the
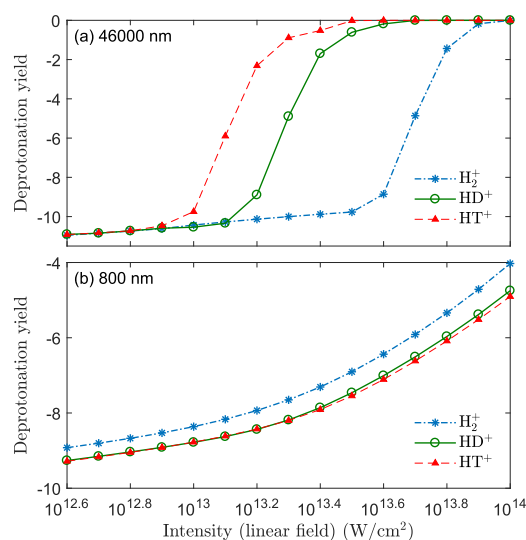
THz laser pulses is remarkably higher than that under the infrared laser pulses. The abrupt enhancement can be seen as a sign of the dynamical regime changing from tunneling to over-barrier dissociation, which is similar to the strong-field over-barrier ionization.[37] According to the second term on the right-hand side of Eq. (19), the field-dressed potential barrier depends on the product of the pulse intensity and the mass asymmetry parameter a_1. It indicates that a_1 being larger would essentially play the role of amplifying the field amplitude for the dissociation. Therefore, the abrupt deprotonation enhancement takes place at relatively lower pulse intensity for heavier asymmetric isotopologues. If the other nucleus is substituted by further heavier nucleus, one might expect a more pronounced deprotonation even in lower pulse intensities.

Next, Fig. 5 shows the dependence of the deprotonation yields on the wavelength of the THz pulse. The corresponding pulse intensities are 9.6×10^{13}, 4.6×10^{13}, and 3×10^{13} W/cm^2 for H_2^+, HD^+, and HT^+, respectively. The intensities are chosen differently to guarantee that the dissociation yields for the three molecules are neither too low nor near saturation when the wavelength varies. As the wavelength increases from 38 000 to 82 000 nm, the dissociation adiabaticity parameter [Eq. (20)] decreases from 0.87 to 0.40 for H_2^+, from 1.45 to 0.67 for HD^+, and from 1.91 to 0.88 for HT^+. One can see that the deprotonation yields as a function of the wavelength decline in general. Such tendency is analogous to the case of strong-field ionization in the tunneling regime.[38]

So far, we have demonstrated the tunneling deprotonation channel by showing the dissociation yields depending on the pulse intensity, wavelength, and the mass asymmetry of the molecular system. In order to gain more insight into the dynamical processes of the nuclear tunneling in the dissociation, we calculate the nuclear momentum distributions for HD^+ driven by the circularly polarized THz pulses. The results for the wavelengths of 38 000 and 52 000 nm are shown in Figs. 6(a) and 6(b), respectively. The corresponding effective vector potentials $-\mathbf{A}_2(t)$ [Eq. (17)] for the deprotonation channel $(D + H^+)$ are also depicted in the nuclear momentum distributions for comparison, respectively. One can observe the streaking patterns that are similar to those observed in the attoclock scheme for studying strong-field tunneling ionization.[27] In general,
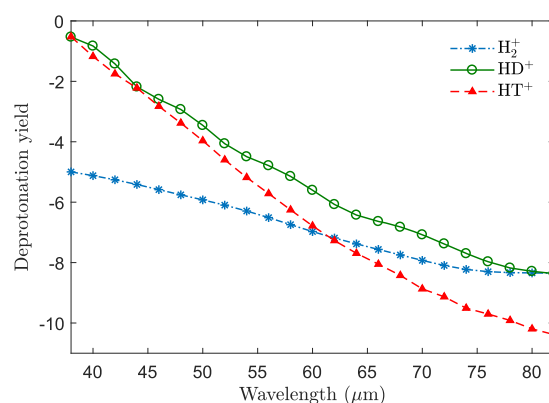

FIG. 4. Deprotonation yield of H_2^+ and its isotopologues as a function of the laser intensity for the three-optical-cycle 46 000-nm circularly polarized THz pulse (a) and the ten-optical-cycle 800-nm circularly polarized infrared pulse (b). The data are shown on logarithmic scales.

FIG. 5. Deprotonation yield of H_2^+ and its isotopologues as a function of the pulse wavelength. The data are shown on logarithmic scales.
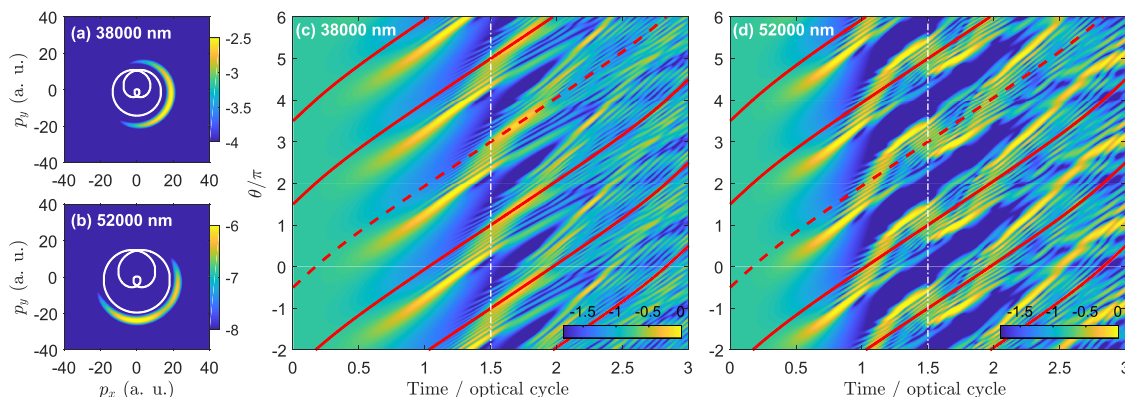
FIG. 6. (a) and (b) The nuclear momentum distributions for the deprotonation of HD$^+$ driven by the three-optical-cycle circularly polarized THz pulses. The white solid curves on the distributions show the effective vector potentials $-\mathbf{A}_2(t)$ for the deprotonation channel. (c) and (d) The time evolution of the angular density distributions of the nuclear wave packets. The red solid and dashed curves indicate the time-dependent field direction. The vertical white dash–dotted line indicates the time when the electric field reaches the peak. The corresponding field amplitude is 0.0256 a.u. for both cases.

we find that the nuclear momentum distributions follow the effective vector potentials, which can be seen as further evidence for the proton tunneling during the interactions. The average nuclear momentum appears to be larger than the corresponding effective vector potential. This might be associated with the nonadiabatic effect that would induce an initial transverse momentum shift of the tunneling particle driven by rotating fields.[28]

Furthermore, one can find a significant offset angle between the peak of the proton distribution and the peak of the vector potential for the case of 38 000 nm shown in Fig. 6(a), while two local maxima appear in the distribution for the case of 52 000 nm shown in Fig. 6(b). To understand the observations, Figs. 6(c) and 6(d) show the time evolution of the angular density distributions of the nuclear wave packets for the two cases, respectively. The solid and dashed curves indicate the direction of the rotating fields, and the vertical dashed-dotted lines indicate the peaks of the electric fields. At the beginning of the interaction, the angular density distribution is isotropic. For the case of 38 000 nm, the nuclear wave packet is gradually localized along a certain direction and rotates during the first optical cycle of the interaction, but there is an offset between the field direction and the localized wave packet. The angular distribution of the wave packet eventually peaks at about 1.68 optical cycles when it is also aligned with the driving field. This process would lead to yield a maximum beyond the peak of the electric field. As a result, the nuclear momentum distribution shown in Fig. 6(a) is significantly deflected from the peak of the vector potential. For the case of 52 000 nm, the localized wave packet oscillates over and behind the rotating field direction. The oscillating density peaks before and after the peak of the electric field, respectively. This would lead to two bursts of the tunneling wave packet and, thus, two local maxima are observed in the nuclear momentum distribution shown in Fig. 6(b).

As we can see, the observation of the proton tunneling in molecular dissociation driven by circularly polarized THz laser pulses is similar to that of strong-field tunneling ionization. On the other hand, however, the underlying dynamics for proton tunneling from molecules is more complex due to the alignment and rotation of the molecule. Nevertheless, the angular streaking of the nuclear momentum distribution indicates that it is possible to control not only the deprotonation yield but also the direction of the emitting proton with the few-cycle circularly polarized THz laser pulses.

IV. CONCLUSION

In conclusion, we have investigated the tunneling mechanism of deprotonation in molecular dissociation driven by circularly polarized THz laser pulses. The numerical results and theoretical analysis show that the tunneling deprotonation is significantly enhanced for asymmetric molecules due to the lowered quasistatic potential barrier associated with the mass asymmetry of the molecules. In particular, the proton tunneling appears much easier for the heavier isotopologues of H$_2^+$ under the same driving pulse. Our results indicate that the tunneling mechanism lowers the necessary pulse intensity for the deprotonation, particularly for molecules with a high degree of mass asymmetry. In addition, we have shown that the emission of the proton can be directed by the vector potential of the driving field and that the alignment and rotation of the molecule would modify the angular distribution the emitting proton.

For the current development of THz lasers, the experimental observation of the tunneling dissociation of molecules driven by THz fields remains challenging. Nevertheless, based on the present theoretical study, we can see that the THz field intensity required for observable tunneling deprotonation could be further lowered if the degree of mass asymmetry becomes larger [see the results in Fig. 4(a)]. Therefore, for those diatomic molecular systems with higher degrees of mass asymmetry (HCl$^+$, for example), there might be chances for experimental observation of the tunneling dissociation at lower THz field intensities.

ACKNOWLEDGMENTS

the public computing service platform provided by the Network and Computing Center of HUST.

AUTHOR DECLARATIONS

Conflict of Interest

The authors have no conflicts to disclose.

Author Contributions

Yidian Tian: Conceptualization (equal); Data curation (lead); Formal analysis (lead); Investigation (lead); Validation (equal); Visualization (equal); Writing – original draft (equal); Writing – review & editing (equal). **Kunlong Liu**: Conceptualization (lead); Formal analysis (equal); Funding acquisition (equal); Investigation (equal); Supervision (equal); Validation (equal); Visualization (equal); Writing – original draft (equal); Writing – review & editing (equal). **Yuchen Wang**: Formal analysis (equal); Investigation (equal); Writing – review & editing (equal). **Yueming Zhou**: Conceptualization (equal); Supervision (equal); Writing – review & editing (equal). **Peixiang Lu**: Conceptualization (equal); Funding acquisition (equal); Writing – review & editing (equal).

DATA AVAILABILITY

The data that support the findings of this study are available from the corresponding author upon reasonable request.

REFERENCES

[1] A. Golan, K. B. Bravaya, R. Kudirka, O. Kostko, S. R. Leone, A. I. Krylov, and M. Ahmed, Nat. Chem. **4**, 323 (2012).

[2] Z.-H. Loh, G. Doumy, C. Arnold, L. Kjellsson, S. H. Southworth, A. Al Haddad, Y. Kumagai, M.-F. Tu, P. J. Ho, A. M. March, R. D. Schaller, M. S. Bin Mohd Yusof, T. Debnath, M. Simon, R. Welsch, L. Inhester, K. Khalili, K. Nanda, A. I. Krylov, S. Moeller, G. Coslovich, J. Koralek, M. P. Minitti, W. F. Schlotter, J.-E. Rubensson, R. Santra, and L. Young, Science **367**, 179 (2020).

[3] Z. Yin, Y.-P. Chang, T. Balčiūnas, Y. Shakya, A. Djorović, G. Gaulier, G. Fazio, R. Santra, L. Inhester, J.-P. Wolf, and H. J. Wörner, Nature **619**, 749 (2023).

[4] A. Kudo and Y. Miseki, Chem. Soc. Rev. **38**, 253 (2009).

[5] T. Hisatomi, J. Kubota, and K. Domen, Chem. Soc. Rev. **43**, 7520 (2014).

[6] J. H. Posthumus, Rep. Prog. Phys. **67**, 623 (2004).

[7] F. He, C. Ruiz, and A. Becker, Phys. Rev. Lett. **99**, 083002 (2007).

[8] A. Giusti-Suzor and F. H. Mies, Phys. Rev. Lett. **68**, 3869 (1992).

[9] L. J. Frasinski, J. H. Posthumus, J. Plumridge, K. Codling et al., Phys. Rev. Lett. **83**, 3625 (1999).

[10] B. D. Esry, A. M. Sayler, P. Q. Wang, K. D. Carnes, and I. Ben-Itzhak, Phys. Rev. Lett. **97**, 013003 (2006).

[11] C. B. Madsen, F. Anis, L. B. Madsen, and B. D. Esry, Phys. Rev. Lett. **109**, 163003 (2012).

[12] A. Natan, M. R. Ware, V. S. Prabhudesai, U. Lev, B. D. Bruner, O. Heber, and P. H. Bucksbaum, Phys. Rev. Lett. **116**, 143004 (2016).

[13] S. Pan, C. Hu, W. Zhang, Z. Zhang, L. Zhou, C. Lu, P. Lu, H. Ni, J. Wu, and F. He, Light: Sci. Appl. **12**, 35 (2023).

[14] K. Liu and I. Barth, Phys. Rev. Lett. **119**, 243204 (2017).

[15] P. H. Bucksbaum, A. Zavriyev, H. G. Muller, and D. W. Schumacher, Phys. Rev. Lett. **64**, 1883 (1990).

[16] A. Giusti-Suzor, X. He, O. Atabek, and F. H. Mies, Phys. Rev. Lett. **64**, 515 (1990).

[17] Z.-C. Li, C. Ruiz, and F. He, Phys. Rev. A **90**, 033421 (2014).

[18] J. R. Hiskes, Phys. Rev. **122**, 1207 (1961).

[19] M. Kübel, M. Spanner, Z. Dube, A. Y. Naumov, S. Chelkowski, A. D. Bandrauk, M. J. J. Vrakking, P. B. Corkum, D. M. Villeneuve, and A. Staudte, Nat. Commun. **11**, 2596 (2020).

[20] J. J. Hua and B. D. Esry, J. Phys. B: At., Mol. Opt. Phys. **42**, 085601 (2009).

[21] J. Meisner and J. Kastner, Angew. Chem., Int. Ed. **55**, 5400 (2016).

[22] P. R. Schreiner, H. P. Reisenauer, F. C. Pickard IV, A. C. Simmonett, W. D. Allen, E. Matyus, and A. G. Csaszar, Nature **453**, 906 (2008).

[23] L. M. Campos, M. V. Warrier, K. Peterfy, K. N. Houk, and M. A. Garcia-Garibay, J. Am. Chem. Soc. **127**, 10178 (2005).

[24] S. H. Bae, X.-X. Li, M. S. Seo, Y. M. Lee, S. Fukuzumi, and W. Nam, J. Am. Chem. Soc. **141**, 7675 (2019).

[25] P. R. Schreiner, J. Am. Chem. Soc. **139**, 15276 (2017).

[26] T. Constantin, B. Gorski, M. J. Tilby, S. Chelli, F. Julia, J. Llaveria, K. J. Gillen, H. Zipse, S. Lakhdar, and D. Leonori, Science **377**, 1323 (2022).

[27] P. Eckle, A. N. Pfeiffer, C. Cirelli, A. Staudte, R. Dörner, H. G. Muller, M. Büttiker, and U. Keller, Science **322**, 1525 (2008).

[28] K. Liu, S. Luo, M. Li, Y. Li, Y. Feng, B. Du, Y. Zhou, P. Lu, and I. Barth, Phys. Rev. Lett. **122**, 053202 (2019).

[29] F. Kelkensberg, G. Sansone, M. Y. Ivanov, and M. Vrakking, Phys. Chem. Chem. Phys. **13**, 8647 (2011).

[30] A. Keller, Phys. Rev. A **52**, 1450 (1995).

[31] T.-Y. Xu and F. He, Phys. Rev. A **88**, 043426 (2013).

[32] K. Liu, Q. Zhang, P. Lan, and P. Lu, Opt. Express **21**, 5107 (2013).

[33] M. D. Feit, J. A. Fleck, Jr., and A. Steiger, J. Comput. Phys. **47**, 412 (1982).

[34] R. Kosloff and D. Kosloff, J. Comput. Phys. **63**, 363 (1986).

[35] K. Liu and I. Barth, Phys. Rev. A **103**, 013103 (2021).

[36] J. T. Paci and D. M. Wardlaw, J. Chem. Phys. **119**, 7824 (2003).

[37] X. M. Tong and C. D. Lin, J. Phys. B: At., Mol. Opt. Phys. **38**, 2593 (2005).

[38] Y. H. Lai, J. Xu, U. B. Szafruga, B. K. Talbert, X. Gong, K. Zhang, H. Fuest, M. F. Kling, C. I. Blaga, P. Agostini, and L. F. DiMauro, Phys. Rev. A **96**, 063417 (2017).